ELSEVIER

Journal of Biomechanics 41 (2008) 1897–1909

JOURNAL OF BIOMECHANICS

www.elsevier.com/locate/jbiomech
www.JBiomech.com

Internal mechanical conditions in the soft tissues of a residual limb of a trans-tibial amputee

S. Portnoy[a], Z. Yizhar[b], N. Shabshin[c], Y. Itzchak[c], A. Kristal[d], Y. Dotan-Marom[d], I. Siev-Ner[d], A. Gefen[a,*]

[a]*Faculty of Engineering, Department of Biomedical Engineering, Tel Aviv University, Israel*
[b]*Faculty of Medicine, Department of Physical Therapy, Tel Aviv University, Israel*
[c]*Department of Diagnostic Imaging, Chaim Sheba Medical Center, Israel*
[d]*Department of Orthopaedic Rehabilitation, Chaim Sheba Medical Center, Israel*

Accepted 31 March 2008

Abstract

Most trans-tibial amputation (TTA) patients use a prosthesis to retain upright mobility capabilities. Unfortunately, interaction between the residual limb and the prosthetic socket causes elevated internal strains and stresses in the muscle and fat tissues in the residual limb, which may lead to deep tissue injury (DTI) and other complications. Presently, there is paucity of information on the mechanical conditions in the TTA residual limb during load-bearing. Accordingly, our aim was to characterize the mechanical conditions in the muscle flap of the residual limb of a TTA patient after donning the prosthetic socket and during load-bearing. Knowledge of internal mechanical conditions in the muscle flap can be used to identify the risk for DTI and improve the fitting of the prosthesis. We used a patient-specific modelling approach which involved an MRI scan, interface pressure measurements between the residual limb and the socket of the prosthesis and three-dimensional non-linear large-deformation finite-element (FE) modelling to quantify internal soft tissue strains and stresses in a female TTA patient during static load-bearing. Movement of the truncated tibia and fibula during load-bearing was measured by means of MRI and used as displacement boundary conditions for the FE model. Subsequently, we calculated the internal strains, strain energy density (SED) and stresses in the muscle flap under the truncated bones. Internal strains under the tibia peaked at 85%, 129% and 106% for compression, tension and shear strains, respectively. Internal strains under the fibula peaked at substantially lower values, that is, 19%, 22% and 19% for compression, tension and shear strains, respectively. Strain energy density peaked at the tibial end (104 kJ/m^3). The von Mises stresses peaked at 215 kPa around the distal end of the tibia. Stresses under the fibula were at least one order of magnitude lower than the stresses under the tibia. We surmise that our present patient-specific modelling method is an important tool in understanding the etiology of DTI in the residual limbs of TTA patients.

Keywords: Prosthesis; Deep tissue injury; Pressure ulcer; Patient-specific finite element model; Rehabilitation

1. Introduction

During lower-extremity amputations, the posterior shank muscles (gastrocnemius and sometimes the soleus) are folded over the distal ends of the truncated bones, and create a muscular flap that is pressed transversely during load-bearing. The majority of trans-tibial amputation (TTA) patients use prostheses on a daily basis. The unnatural mechanical conditions that result from the interaction between the soft tissues of the residual limb and the prosthetic socket often lead to pain, blisters, edema, pressure ulcers and sometimes flap necrosis and osteomyelitis (Lyon et al., 2000; Mak et al., 2001). The surgically sharpened tibial end can cause critical mechanical loads in the tissues underneath, which may eventually lead to flap ulceration (Henrot et al, 2000). It has been long known that tissue loads are higher internally near bony prominences than at the skin surface (Le et al., 1984). However, only recently, a perilous injury condition named

*Corresponding author. Tel.: +972 3 640 8093; fax: +972 3 640 5845.
E-mail address: gefen@eng.tau.ac.il (A. Gefen).

0021-9290/$ - see front matter © 2008 Elsevier Ltd. All rights reserved.
doi:10.1016/j.jbiomech.2008.03.035

"deep tissue injury" (DTI) was introduced. Deep tissue injury is a muscle lesion under intact skin (Black, 2005; Ankrom et al., 2005; Agam and Gefen, 2007). In TTA patients, DTI results from compression of the muscle flap by the truncated bones against the socket. Knowledge of DTI etiology is yet to be established; however, the undisputed factors are pressure-related ischemia together with excessive soft tissue deformation (Bouten et al., 2003; Gefen, 2008). The onset of DTI strongly depends on the geometrical and biomechanical characteristics of the bone–muscle interface (Gefen, 2007a, b), which differ widely across individual TTA patients due to different surgical techniques, level of amputation, muscle atrophy and scarring (Portnoy et al., 2007). Since approximately 80% of lower limb amputees suffer peripheral vascular disease, diabetes or both (Kulkarni et al., 2006), the neuropathy associated with these diseases prevents patients from detecting pain and injury to their residual limb.

Presently, there is paucity of information on mechanical conditions in the residual limb during load-bearing. Since it is not feasible to invasively measure internal strains and stresses in the muscle flap of TTA patients, computational models must be incorporated. Finite-element (FE) modelling was used by several research groups to create two-dimensional (2D) or three-dimensional (3D) residual limb models, for determining pressure and shear distributions at the skin surface (Reynolds and Lord, 1992; Sanders and Daly, 1993; Zhang and Roberts, 2000). However, FE analysis was never before utilized for characterizing internal strains and stresses in muscle flap of residual limbs, excluding our recent study (Portnoy et al., 2007) which employed a 2D real-time approach. Knowledge of internal mechanical conditions in the 3D residual limb is very likely to prove useful in preventing DTI in TTA patients, as well as in aiding in surgical planning and rehabilitation, thus improving the health and comfort of the active amputee.

Consequently, our goal was to characterize the mechanical conditions in a muscle flap of a TTA patient during static load-bearing. We specifically aimed at developing a technique that, ultimately, will be able to identify the risk for DTI in individual patients and improve prosthetic fitting based on integration of MRI and interface pressure measurements in a patient-specific FE model.

2. Methods

Two thin (0.3 mm) and flexible pressure-sensing mats based on piezoresistive sensors were designed specifically for this project, jointly by our Musculoskeletal Biomechanics Laboratory (AG) and Sensor Products Co. (NJ, USA). Dimensions of the mats were selected according to anthropometric data of lengths and circumferences of residual limbs of TTA patients (Sanders et al., 2005). The posterior pad consists of 175 pressure sensors, where the proximally located part is wider (rectangular array of 15×5 sensors) than the distally located part (10×10 rectangle) to adequately envelope the upper shin (Fig. 1a, b). The anterior pad consists of 150 sensors (6×25 rectangle) and is long enough to be folded over the distal end of the residual limb (Fig. 1a, c). The area of one sensor is 1.024 cm^2 and its measurement capacity is ~700 kPa. The accuracy, repeatability, hysteresis and non-linearity of sensors are ±10%, ±2%, ±5% and ±1.5%, respectively. Sensors and cables were shielded to minimize electrical noise and potential effects of in-socket temperature and humidity. Together, the sensor arrays were sampled at 19 Hz. Data were processed using commercial software (Tactilus, version 3.1.12, Sensor Products Co., NJ, USA). The pressure-sensing mats were placed

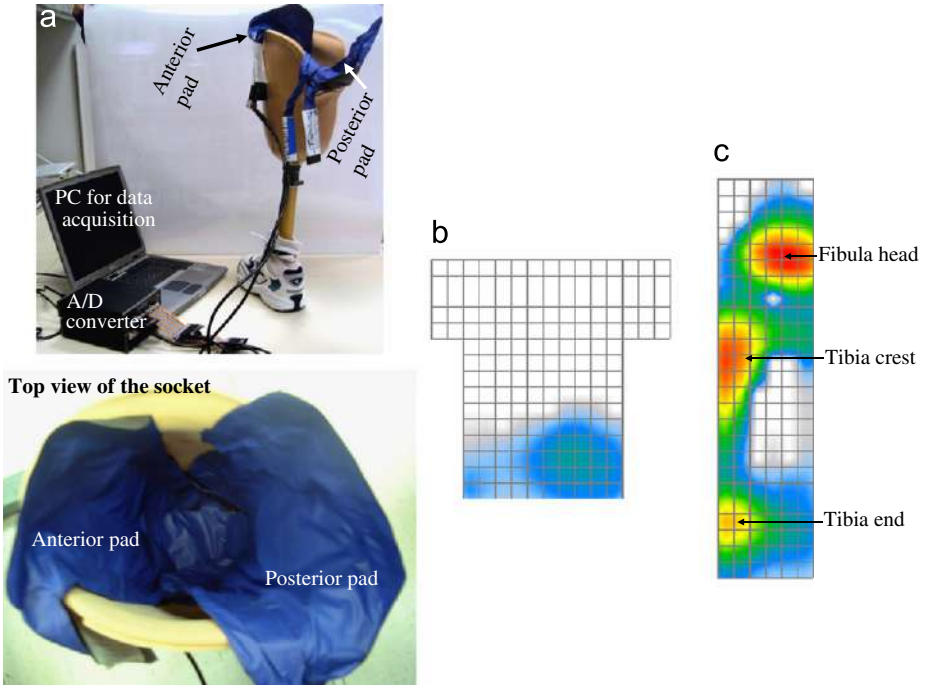

Fig. 1. The pressure measurement system (a) and an example of a pressure distribution recorded around the residual limb during static load-bearing by (b) the posterior mat and (c) the anterior mat, folded at the distal end of the residual limb. The peak pressure value (red spots at the fibular head and tibial crest) was 65 kPa.

between the prosthetic socket and residual limb to obtain static interface pressure diagrams (Fig. 1). Though it was ideal to acquire pressure data simultaneously with the MRI studies described below, electronic interferences prevented this, so pressure data were acquired before the MRI trials.

The MRI studies were carried out at an open MRI (Fig. 2), which consists of two vertical magnets with a space between them for access during surgical procedures (field intensity 0.5 T, spatial resolution 0.1 mm, slice thickness 4 mm, images were T1-weighted, phase field-of-view 100%, "Signa SP" model, General Electric Co., CT, USA). Herein, we employed the space between the magnets to study the internal anatomy of the residual limb while the TTA patient stood between them (Fig. 2). We recruited a healthy-traumatic active TTA female subject (age 29, height 1.69 m, weight 50 kg) with no history of diabetes mellitus or symptoms of peripheral neuropathy. Helsinki approval (#4302/06 from Sheba Medical Center, Israel) and informed consent were obtained. The patient complained about daily pain and discomfort at the distal end of her residual limb and at the fibula head region, while using her prosthesis. She also complained about frequent skin injuries at the distal residual limb.

A plaster cast was created from the residual limb pre-trial (Fig. 3a), and used as a non-metallic substitute for the patient's own socket during MRI scans. Two scan sequences were acquired: (i) when the patient was donning the plaster socket with no externally applied load (Fig. 2a), and (ii) during static external loading of the socket by the patient's body weight (Fig. 2b). Two thin piezoresistive force sensors (accuracy $\pm 5\%$, capacity 440 N, FlexiForce, Tekscan Co. MA, USA) were placed between the socket and the MRI's patient table to verify continuous loading on the residual limb.

The 3D surfaces of bone and muscle tissues were obtained from coronal and transversal MRI scans (Fig. 3b). The MRI scans were loaded into parallel planes and contours of the bones and muscle were manually drawn per each slice and lofted into 3D bodies (Fig. 3c) by means of a solid modelling software (SolidWorks 2005, SolidWorks, MA, USA). The 3D reconstruction of the unloaded residual limb was imported to an FE solver (ABAQUS version 6.6, SIMULIA, RI, USA) for non-linear large-deformation strain/stress analyses (Fig. 4a).

The model included the tibia and fibula bones, the muscle flap, skin and the socket. Vertical movement of the bones during weight-bearing was measured by comparing the 3D reconstructions of the unloaded and loaded MRI scans; we then applied these bone movements as displacement boundary conditions for the FE model. The external cast surface was constrained for all translations. The friction coefficient between the skin and cast was set to 0.7 (Sanders et al., 1998). The cast was assumed to be homogeneous isotropic and linear-elastic material, with elastic modulus of 1 GPa and Poisson's ratio of 0.3. Since the cast acts as a rigid container for the residual limb (e.g. it is over 4-orders-of-magnitude stiffer than muscle tissue; Palevski et al., 2006), we referred to it as such. Bones were considered rigid, and all soft tissues were assumed to be homogeneous, isotropic and incompressible. Skin was characterized using an energy function based on the strain energy function by James et al. (1975) assuming incompressibility (Reihsner et al., 1995; Lanir et al., 1990):

$$W_{\text{skin}} = C_{10}(I_1 - 3) + C_{11}(I_1 - 3)(I_2 - 3) \tag{1}$$

where W_{skin} is the skin's strain energy per unit of reference volume, and the invariants of the principal stretch ratios are $I_1 = \Sigma_{i=1}^{3}\lambda_i^2$ and $I_2 = \Sigma_{i=1}^{3}\lambda_i^{-2}$, where λ_i are the principle stretch ratios, and the material constants are $C_{10} = 0.4$ kPa and $C_{11} = 82$ kPa (Hendriks et al., 2003). The constitutive behavior of muscle tissue was also represented using an energy function, but viscoelastic stress relaxation, which is considered important in static load-bearing (Palevski et al., 2006; Linder-Ganz et al., 2007), was incorporated. Specifically, following the work of Linder-Ganz et al. (2007), the instantaneous stress response of muscle was represented using a neo-Hookean strain energy function:

$$W_{\text{muscle}} = \frac{G^{\text{ins}}}{2}(I_1 - 3) \tag{2}$$

where $G^{\text{ins}} = 8.5$ kPa is the short-term transverse shear modulus of non-preconditioned muscle tissue (Palevski et al., 2006). Viscoelasticity was then considered by means of a Prony series expansion:

$$S(t) = (1-\delta)\frac{\partial W_{\text{muscle}}}{\partial E} + \int_0^t \delta \frac{\partial W_{\text{muscle}}}{\partial E} e^{-(t-\xi)/\tau} d\xi \tag{3}$$

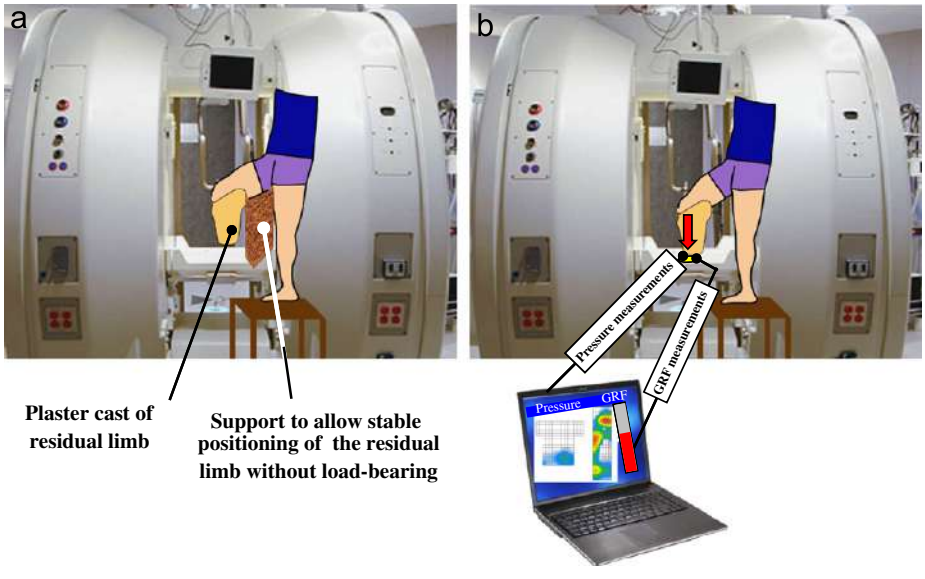

Fig. 2. A scheme of the imaging configuration at the open-MRI, where the residual limb of the subject is (a) unloaded and (b) statically loaded. Ground reaction force (GRF) measurements were taken by means of two force sensors located between the bottom of the socket and the MRI's patient table, to ensure continuous load transfer through the residual limb while it was scanned by MRI at the load-bearing experimental mode. The contact pressure distribution around the residual limb was acquired before the MRI scan.

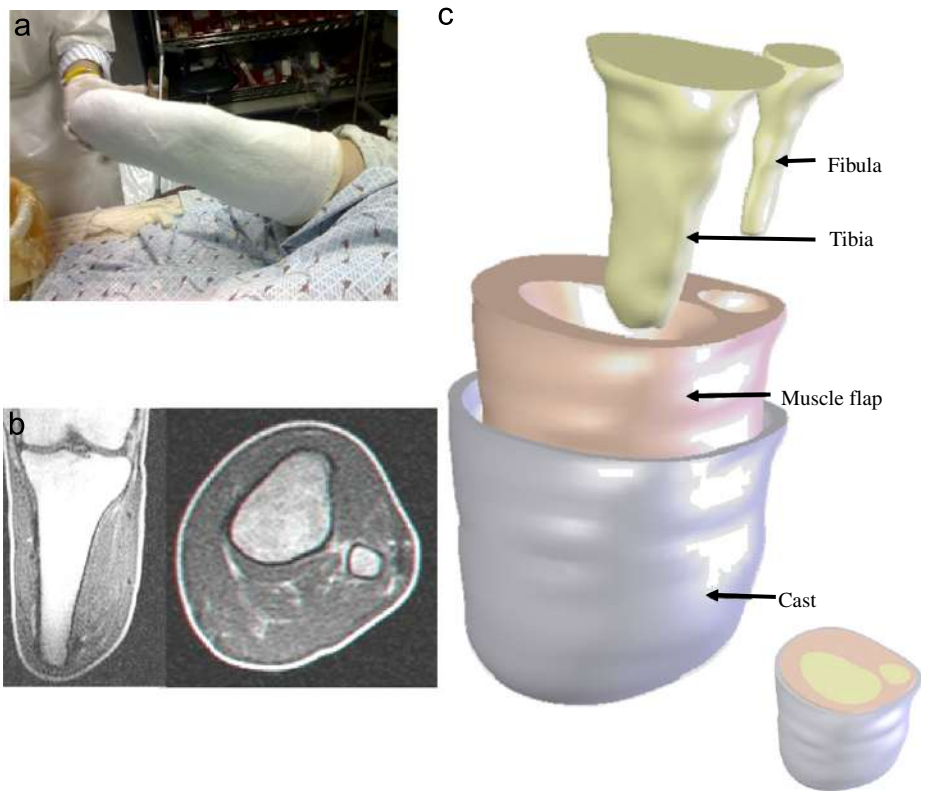

Fig. 3. The process of patient-specific finite-element (FE) modelling: (a) After creating a plaster cast of the residual limb of a TTA patient, (b) Coronal and transverse MR images were acquired in an open MRI at a static posture, with and without load-bearing (as depicted in Fig. 2). (c) Then, a three-dimensional solid model of the residual limb was created from the MR images (SolidWorks, 2005), for export to the FE solver.

where S is the second Piola–Kirchhoff stress, E is the Green–Lagrange strain, τ is the relaxation time constant and $\delta = 50\%$ is the percentage difference between tissue moduli at the instant of deformation and at the asymptotic response (Linder-Ganz et al., 2007). Since we only account for tissue stress distributions at long terms (considering that MRI scans took several minutes to acquire but most stress relaxation in transversally loaded skeletal muscle tissue already occurs within ~20 s; Palevski et al., 2006), muscle stresses can be approximated as $S \cong (1-\delta)\partial W/\partial E$.

The "rigid" bones were meshed with 3071 4-node quadrilateral surface elements ("SFM3D4" in ABAQUS) which cannot deform and are not assigned with mechanical properties. Muscle tissue was meshed with 27470 second-order 10-node modified quadratic tetrahedron elements ("C3D10M"). "No slip" conditions were set at the interfaces between muscle and bone. The outer muscle layer was configured as skin tissue, and meshed with 2136 6-node triangular membrane elements ("M3D6"). The cast was meshed with 3744 "C3D10M" elements. The mesh density was tested in preliminary simulations, where it was found that denser meshes increased the runtime but had negligible effect on the strain/stress measure outcomes. At its final configuration, the runtime of the model was approximately 12 h using pentium-class workstation equipped with 1 GB RAM and designated graphic processor board.

The FE model was first analyzed for distributions of internal principal strains and maximal shear strains in the muscle flap. We also calculated the strain energy density (SED) distribution in the flap, as a useful scalar measure of the intensity of tissue loading. We further calculated distributions of principal stresses, maximal shear stresses and von Mises stresses, which are reported as Cauchy stresses (σ)

$$\sigma_{jr} = F_{ij} S_{ik} J^{-1} F_{rk} \tag{4}$$

where F is the deformation gradient tensor and $J = \det(F)$.

3. Results

The patient had relatively thin and muscular residual limb, and accordingly, the MRI scan did not reveal fat tissue (Fig. 3b, c). Consequently, fat was not modelled herein. Anatomical dimensions of the residual limb are listed in Table 1, with respect to those of a group ($N = 5$) of previously studied TTA patients (Portnoy et al., 2007). These data show that the muscle flap of the present patient was considerably narrower and thinner than of other patients.

A 0.9 ± 0.1 mm downward displacement of the bones relative to the socket was measured in the residual limb during load-bearing, by comparing between MRI scans of the non-weight-bearing versus weight-bearing using the technique of Linder-Ganz et al. (2007). Hence, a 0.9 mm downward displacement was imposed on the bones in the FE model, resulting in a 3D distribution of soft tissue deformations (Fig. 4b). As the truncated bones were pushed against the cast, underlying muscle tissue was compressed, whereas more distant muscle tissue was pushed upwards, toward the knee (Fig. 4b). Sliding of the skin against the cast peaked at 0.61 mm under the tibia (Fig. 4c). Interface limb–socket pressures, calculated from the FE model, peaked at 65 kPa, and were in excellent agreement with the experimental pressure measurements that

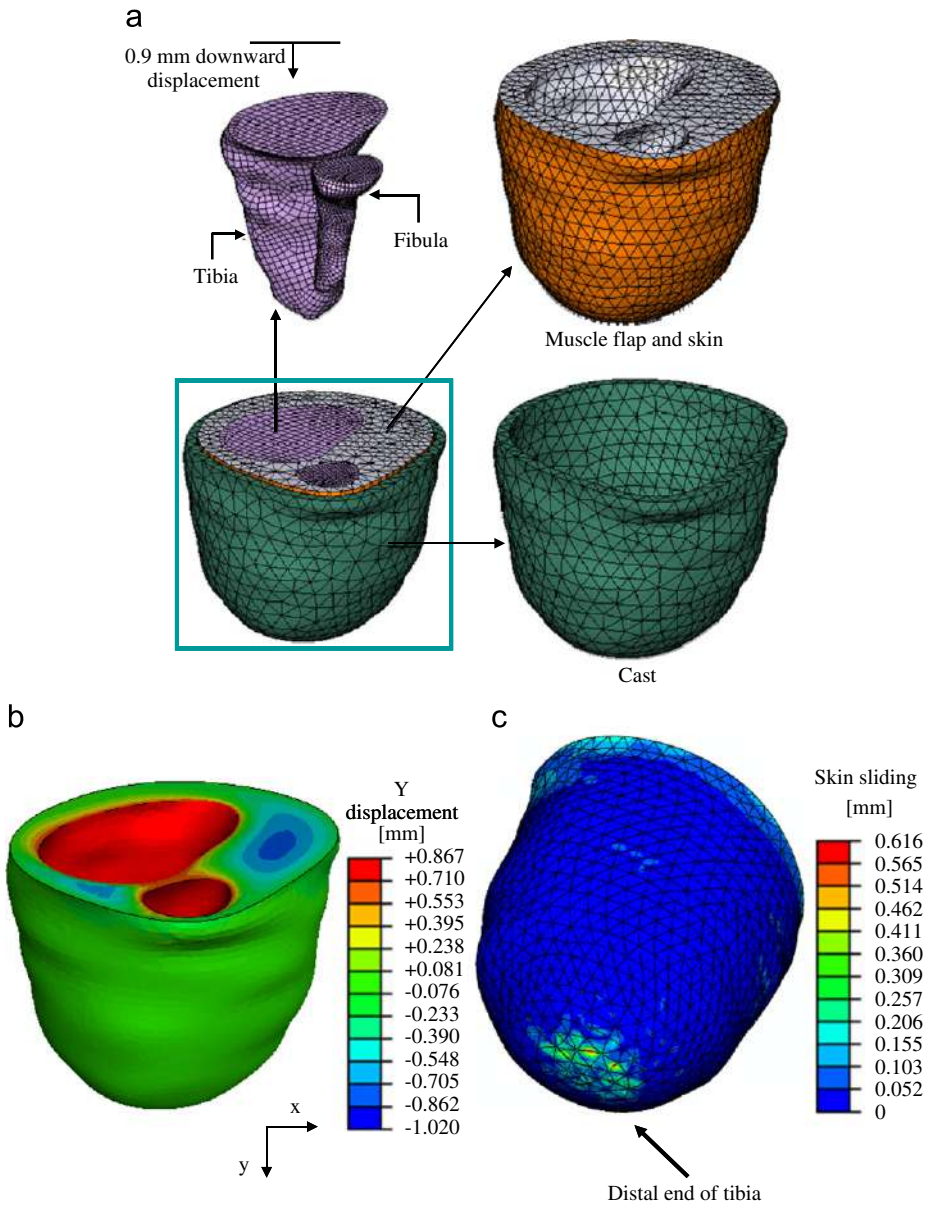

Fig. 4. Finite-element (FE) meshing and displacement boundary conditions imposed on the tibia and fibula bones: (a) The FE meshes of the tibia and fibula, muscle and skin, and the plaster cast. (b) Distribution of tissue displacements in the vertical direction after a downward movement of ~1 mm was imposed on the truncated bones, whereas the outer cast surface was constraint for all translations. (c) Sliding of the skin (mm). It is shown that displacements of skin elements occur mainly at the proximal and distal ends of the FE model.

Table 1
Residual limb geometrical characteristics measured from an MRI scan of the trans-tibial amputation (TTA) patient studied herein, compared with residual limb geometrical characteristics obtained from X-rays of a group of 5 TTA patients in a previous study (Portnoy et al., 2007)

Residual limb characteristics	Tibia length (cm)	Fibula width (cm)	Posterior muscle width (cm)	Minimal flap thickness (cm)
TTA patient from current study	12.76	1.23	1.1*	0.22*
TTA patients from previous study*	13.26±3.27	1.35±0.38	3.9±0.94	2.48±1.51

It is shown that the muscle flap of the present patient is significantly narrower and thinner with respect to that of other TTA patients.
*$p \ll 0.01$ in a 2-tails, unpaired t-test.

fluctuated ±10 kPa around this value with postural sways (Fig. 1). Shear stresses on the skin peaked at 51.9 kPa under the tibia.

The internal strain distributions at the distal ends of the tibia and fibula are shown in Figs. 5 and 6, respectively. Principal compression and tension strains, SED and

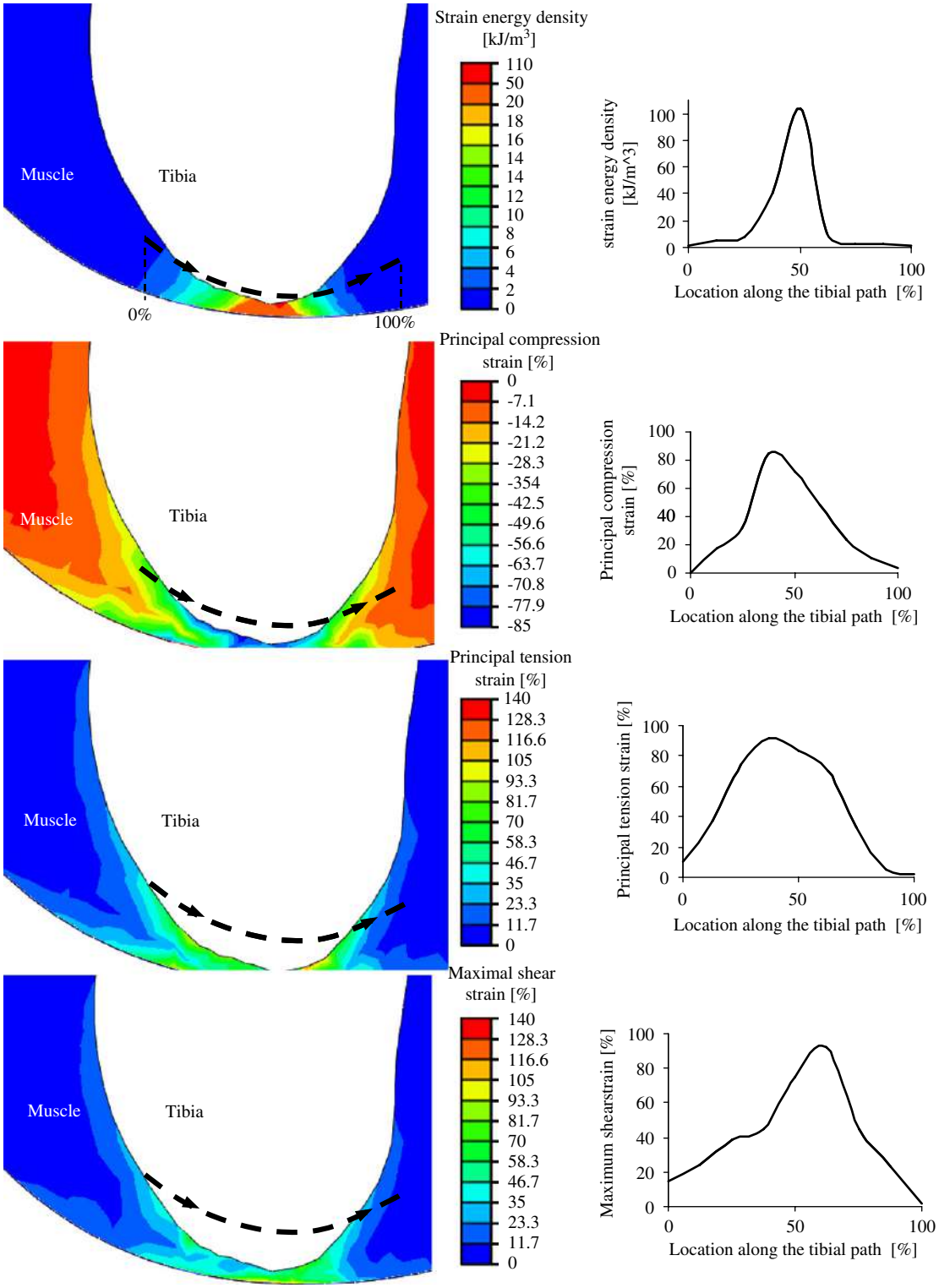

Fig. 5. The internal strain distribution at the distal end of the tibia. Strain energy density, principal compression and tension strains and maximal shear strains are plotted along a path below the tibia.

maximal shear strains were plotted along paths below the tibia and fibula. The SED peaked directly at the distal tibial end ($104\,kJ/m^3$) and laterally to the distal fibular end, where it was at least 2-orders-of-magnitude lower than under the tibia. Principal compression and tension strains and maximal shear strains peaked directly at the distal tibial end and laterally to the distal fibular end. Peak internal strains under the tibia were 85%, 129% and 106% for compression, tension and shear, respectively. Peak internal strains under the fibula were substantially lower: 19%, 22% and 19% for compression, tension and shear, respectively.

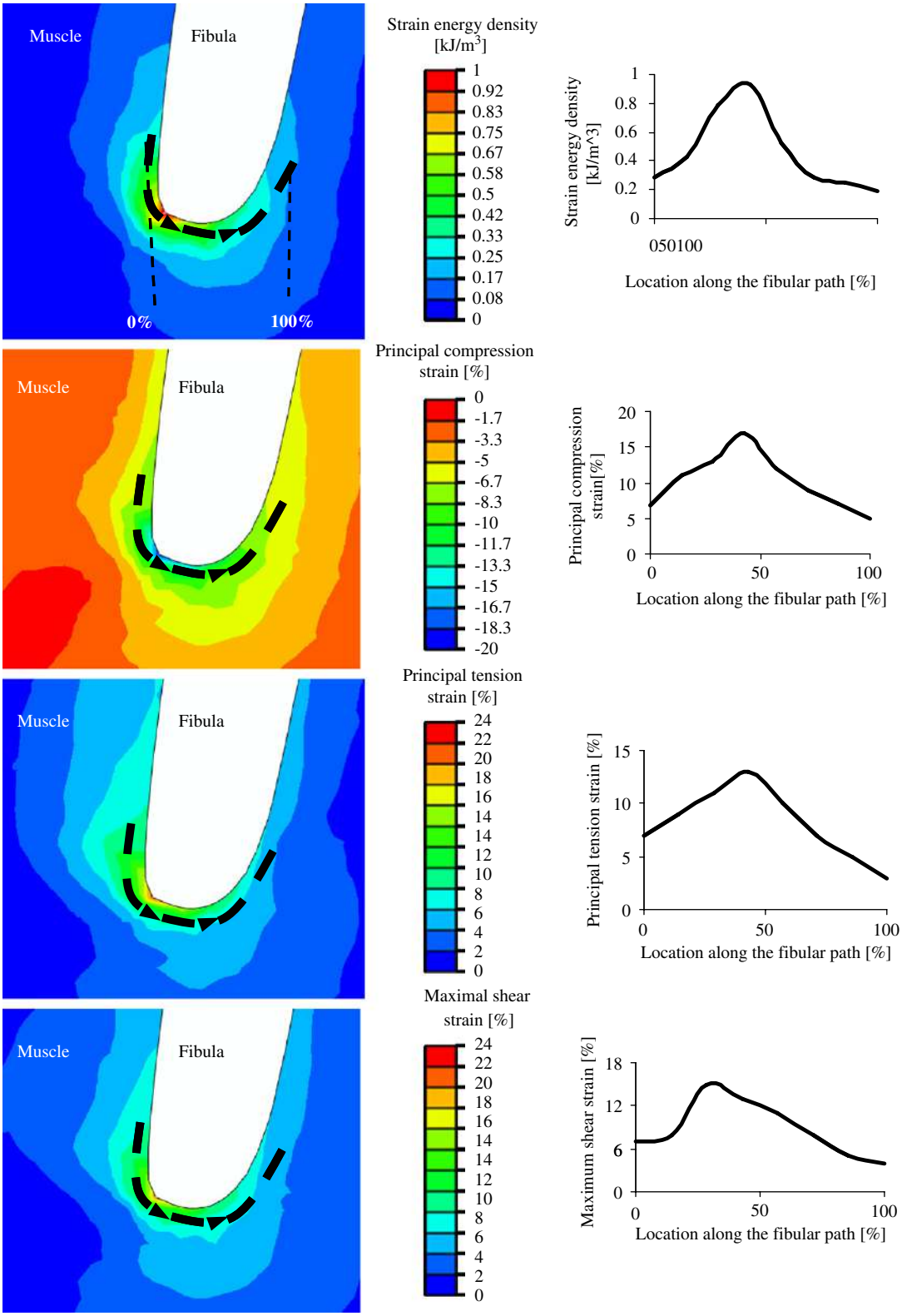

Fig. 6. The internal strain distribution at the distal end of the fibula. Strain energy density, principal compression and tension strains and maximal shear strains are plotted along a path below the fibula.

The internal stress distributions at the distal tibial and fibular ends are presented in Figs. 7 and 8, respectively. The von Mises stresses, principal compression and tension stresses and the maximal shear stresses were plotted along a path below each bone. Stress distributions in the muscle flap corresponded to strain distributions, i.e. all stresses peaked directly at the distal tibial end and laterally to the distal fibular end (Fig. 7). Stresses under the fibula were at

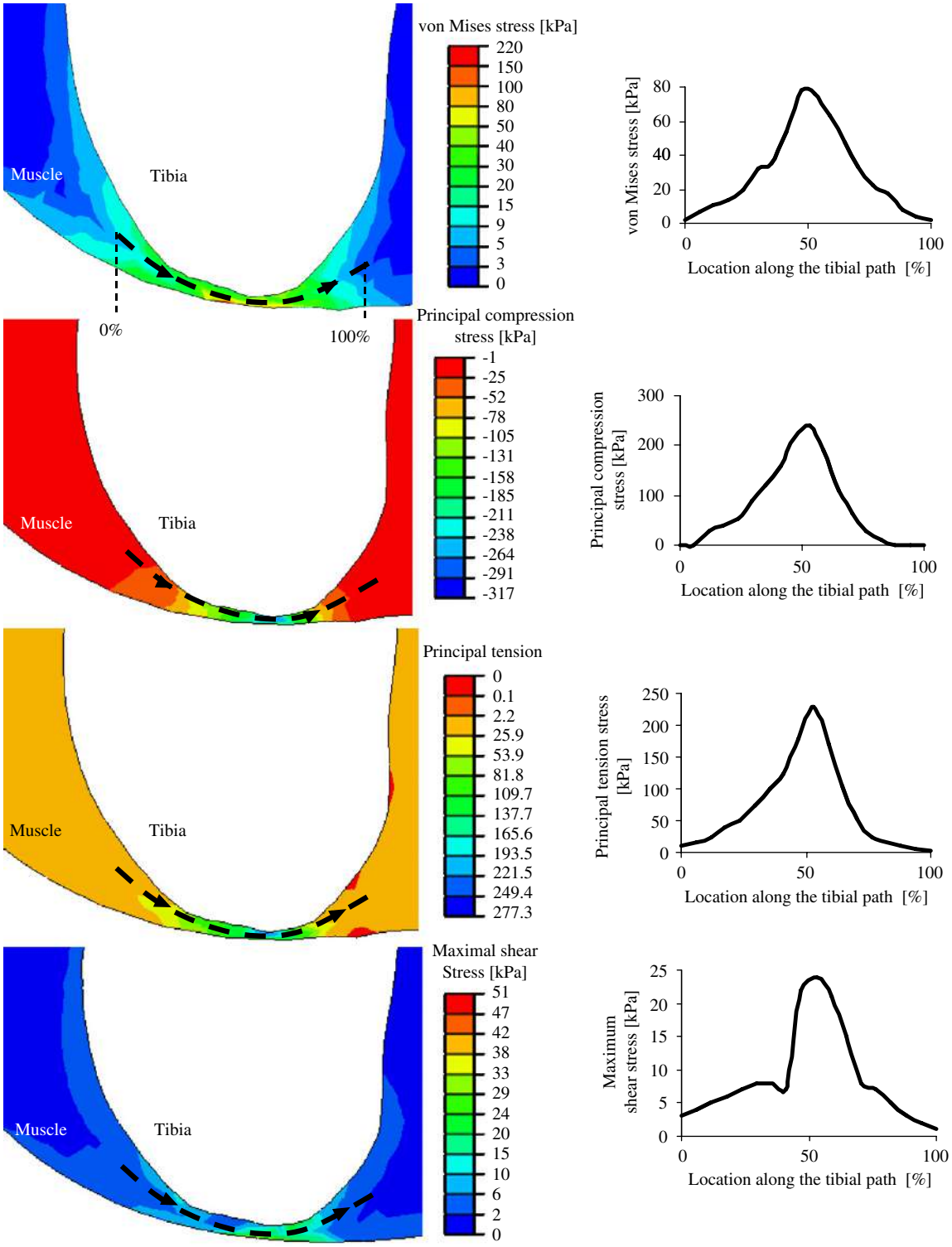

Fig. 7. The internal stress distribution at the distal end of the tibia. Von Mises stresses, principal compression and tension stresses and maximal shear stresses are plotted along a path below the tibia.

least one-order-of-magnitude lower than under the tibia. The von Mises stress concentrations created in the muscle flap by the end of the truncated tibia (peak 215 kPa) is shown in Fig. 9.

Overall, the highest muscle flap strains, SED and stresses were found directly under the distal tibial end (Figs. 5, 7 and 9 and Table 2). For example, peak muscle compression stresses under the tibia (Fig. 7) were over 4-fold greater than skin interface pressures at that location. We conclude that the stress concentrating effect of bony prominence, which was already identified as a key contributor to the formation of pressure ulcers and DTI (Gefen, 2007a, b), is

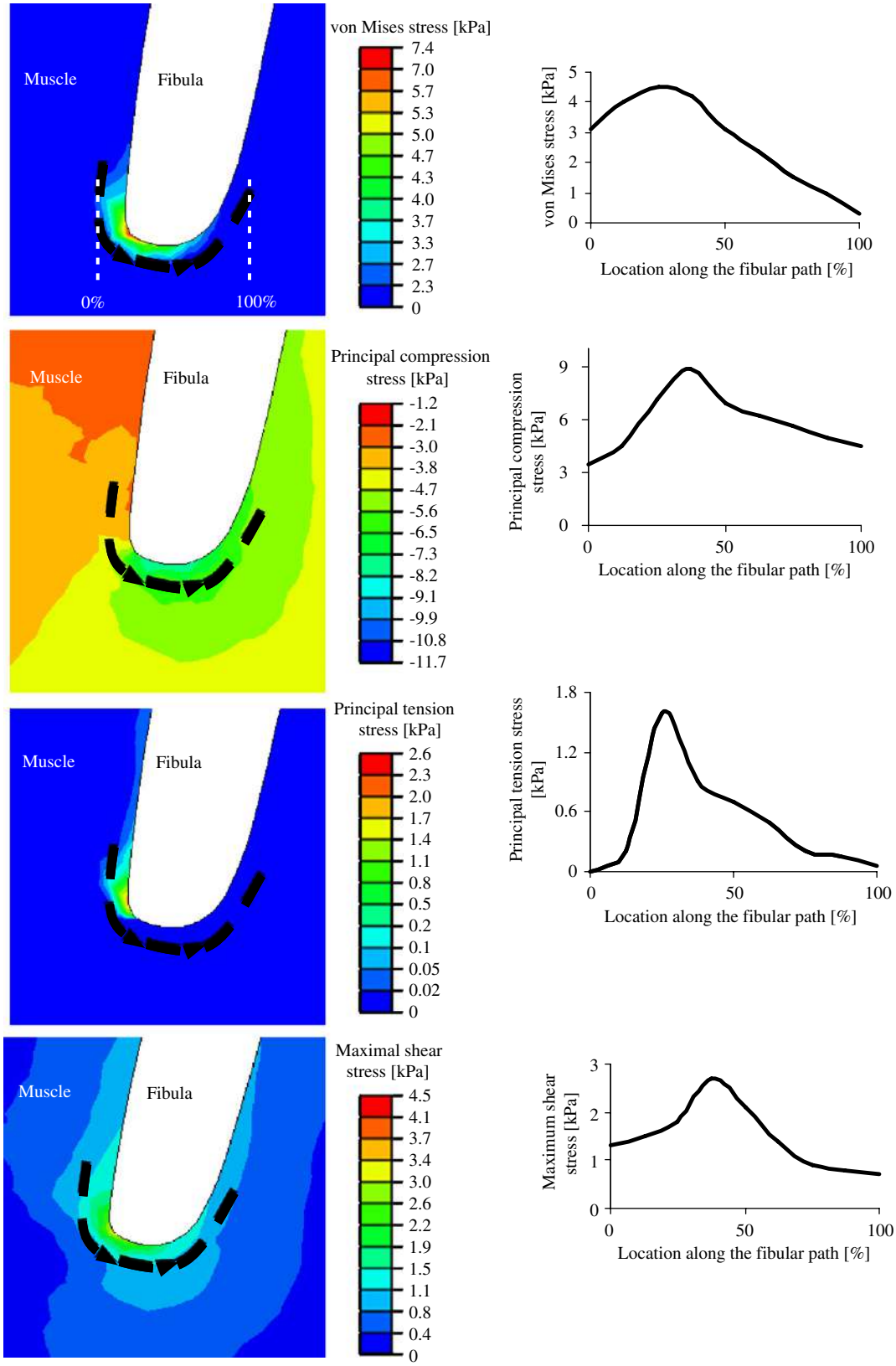

Fig. 8. The internal stress distribution at the distal end of the fibula. Von Mises stresses, principal compression and tension stresses and maximal shear stresses are plotted along a path below the fibula.

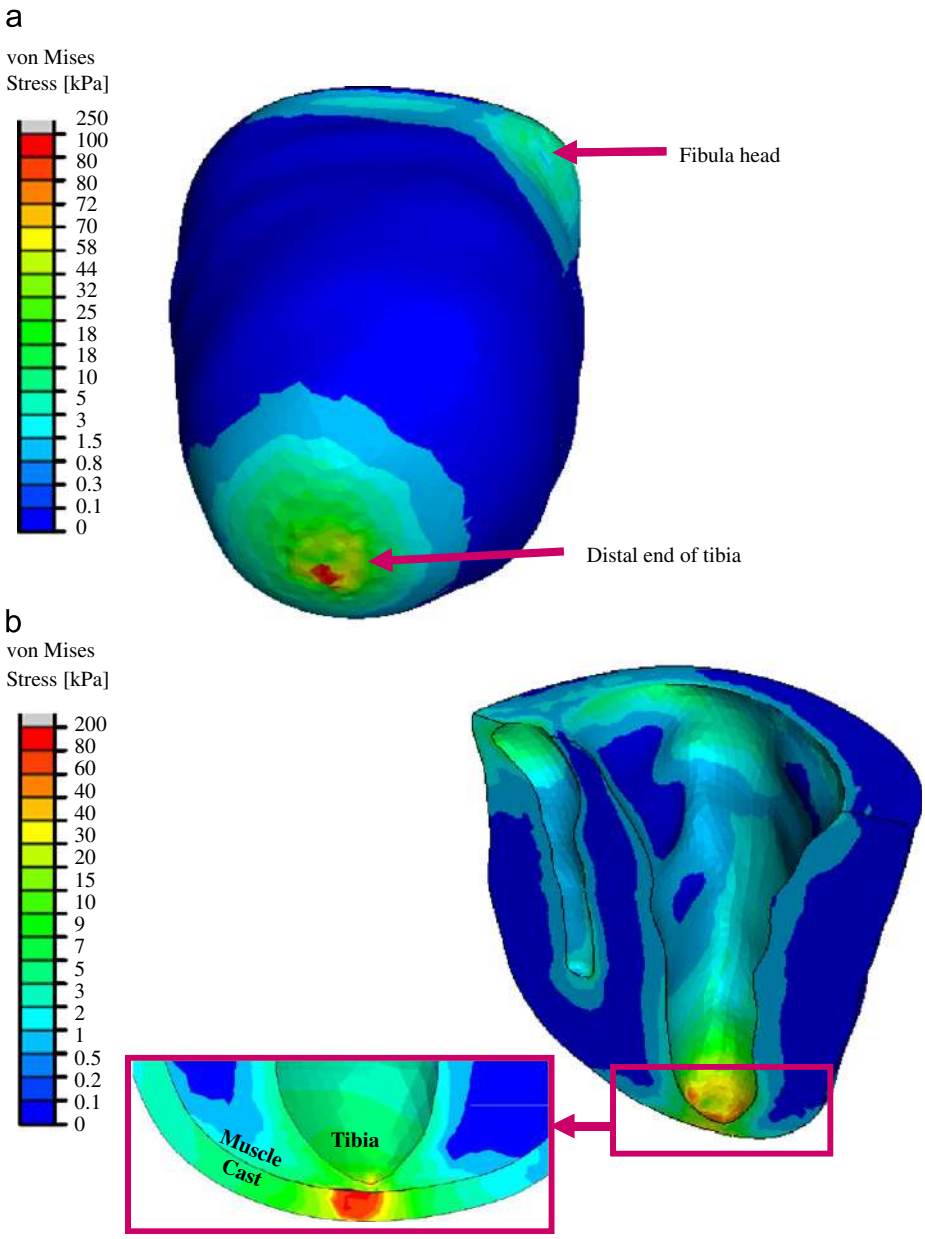

Fig. 9. The von Mises stress distribution in the residual limb of a trans-tibial amputee during static loading: (a) Stresses on the surface of the residual limb. (b) Stresses in a coronal cross-section through the truncated bones, with views on the muscle tissue surrounding the bones. A magnified region under the truncated tibia, in the bottom frame, shows elevated von Mises stresses in the muscle flap and the interaction with the hard cast.

Table 2
Calculated strains, strain energy densities and stresses at important anatomical sites

Parameter	Tibial tuberosity	Tibia end	Popliteal depression	Fibula head	Fibula end
Principal compressive strain (%)	7	85	0.2	0.2	19
Principal tensile strain (%)	6.9	129	1.8	4.5	22
Maximal shear strain (%)	8.9	106	1	1.5	19
Strain energy density (kJ/m^3)	0.04	104	0.01	0.02	1
Principal compressive stress (kPa)	3.3	240	1.1	4	8.9
Principal tensile stress (kPa)	1.4	263	0.7	7	2.2
Maximal shear stress (kPa)	0.5	23	0.4	3.2	3.3
von Mises stress (kPa)	1.3	215	0.9	6.4	7.4

particularly strong under the truncated tibia of the patient studied herein.

4. Discussion

This study introduces a new experimental-computational technique for quantifying internal mechanical conditions in residual limbs of TTA patients. Over the last two decades, efforts were invested in drawing FE models closer to resembling the actual residual limb, anatomically and mechanically. Childress and colleagues were the first to confront this challenge (Steege et al., 1987). Since then, linear elastic simplified 2D models have evolved into geometrically accurate non-linear 3D models, bearing fewer assumptions regarding mechanical behavior of tissues and contact conditions. Some models included slip and friction at the limb–socket interface (Lee et al., 2004; Zachariah and Sanders, 2000; Zhang et al., 1995). Others considered inertial effects (Jia et al., 2004) and non-linear properties of soft tissues (Tonuk and Silver-Thorn, 2004). Anatomically accurate FE model of a TTA residual limb was created for surface temperature analysis (Peery et al., 2006). However, so far, no study combined non-linear characterization of soft tissues in an anatomically accurate 3D model of the residual limb, while considering large deformations and friction between the skin and socket. This is the first study that considers these features simultaneously, and, importantly, it is the first to report internal conditions in the muscle flap that are required for pressure ulcer and DTI etiological research.

We found strain and stress concentrations in the flap under the tibial end, demonstrating the perilous condition of muscle tissue in the loaded residual limb. Nevertheless, the residual limb of our TTA patient is slim and muscular, and no significant fat tissue partitioned between the muscle flap and hard inner surface of the cast. Moreover, as indicated in Table 1, the flap thickness of her residual limb is less than 10% and the posterior muscle width is ~3-fold smaller than those of residual limbs of TTA patients we previously studied (Portnoy et al., 2007). It is therefore likely that this patient is exposed to relative higher strain/stress levels, and her complains about discomfort and pain at the distal residual limb further support this.

The peak principal compression strain in the muscle flap of our TTA patient was slightly higher than physiological compression levels previously reported for the gluteus muscle of healthy subjects during sitting (Linder-Ganz et al., 2007). However, the peak principal tensile strain and shear strain found in her flap were ~5-fold the physiological levels in Linder-Ganz et al. (2007). It has been widely reported that the residual limb is subjected to high external shearing forces at the limb–socket interface (Zhang et al., 1998, Sanders and Daly, 1993; Quesada and Skinner, 1991). It is also known that with increasing shear, the pressure necessary to occlude skin blood flow drops as low as half the baseline value (Bennett et al., 1979; Linder-Ganz and Gefen, 2007). Hence, although compression strains found in the muscle flap of our subject appeared to be at physiological levels, the high tensile and shear strains might be a risk for tissue viability.

We included SED calculations, which were previously used to predict tissue breakdown, e.g. of kidney (Snedekera et al., 2005.). In lack of an SED-based injury threshold for skeletal muscle, we cannot predict the risk for tissue breakdown in the patient examined herein, but hopefully, in the future, such SED threshold will become available. This will require animal studies where tissue viability is monitored under compound (compression + tension + -shear) loading. An initial work to establish tissue injury threshold for skeletal muscle (considering only compression loading at this stage) has already started in our laboratory (Linder-Ganz et al., 2006). The pressure ulcer research group in Eindhoven University of Technology is also progressively acting to provide such data (Stekelenburg et al., 2006a, b, 2007).

The limitations of our study are mostly related to the mechanical properties assigned to the muscle flap. We did not take into account effects of muscle tonus or scars on the tissue's mechanical behavior, in lack of appropriate constitutive data. In TTA patients, the distal end of the muscle flap is surgically attached to the distal tibial end but for the purpose of FE analysis, bone–muscle interface nodes were assigned "tie" connection, and no relative motion was allowed. Another limitation of our clinical trial is the use of a plaster substitute for the prosthetic socket. In rehabilitation centers, sockets are rectified "custom-made" to divert pressures from sensitive areas to more tolerant areas (Silver-Thorn and Childress, 1996; Fergason and Smith, 1999). Since these modifications were not performed, we may have somewhat overestimated tissue loading in a custom prosthetic socket. Additionally, considering that our sensing mats were very thin (0.3 mm) and completely flexible, effects of the presence of the sensor layer on measured pressure data were assumed negligible. To conclude, we surmise that our approach is adequate for characterizing internal strains/stresses in residual limbs, and that its contribution in understanding pressure ulcers, DTI and flap necrosis etiologies is significant.

Conflict of interest statement

None.

Acknowledgments

The authors appreciate the help of Mr. Eran Linder-Ganz for assisting in SolidWorks and ABAQUS. Funding of this research is provided by the Chief Scientist of the Israeli Ministry of Health (A.G., Z.Y.) and by the Nicholas and Elizabeth Slezak Super Center for Cardiac Research and Biomedical Engineering (AG).

References

Agam, L., Gefen, A., 2007. Pressure ulcers and deep tissue injury: a biomechanical perspective. Journal of Wound Care 16, 336–342.

Ankrom, M.A., Bennett, R.G., Sprigle, S., Langemo, D., Black, J.M., Berlowitz, D.R., Lyder, C.H., 2005. Pressure-related deep tissue injury under intact skin and the current pressure ulcer staging systems. Advances in Skin and Wound Care 18, 35–42.

Bennett, L., Kavner, D., Lee, B.K., Trainor, F.A., 1979. Shear vs pressure as causative factors in skin blood flow occlusion. Archives of Physical Medicine and Rehabilitation 60, 309–314.

Black, J.M., 2005. Moving toward consensus on deep tissue injury and pressure ulcer staging. Advances in Skin and Wound Care 18, 415–421.

Bouten, C.V., Oomens, C.W., Baaijens, F.P., Bader, D.L., 2003. The etiology of pressure ulcers: skin deep or muscle bound? Archives of Physical Medicine and Rehabilitation 84, 616–619.

Fergason, J., Smith, D.G., 1999. Socket considerations for the patient with a transtibial amputation. Clinical Orthopaedics and Related Research 361, 76–84.

Gefen, A., 2007a. Risk factors for a pressure-related deep tissue injury: a theoretical model. Medical and Biological Engineering and Computing 45, 563–573.

Gefen, A., 2007b. The biomechanics of sitting-acquired pressure ulcers in patients with spinal cord injury or lesions. International Wound Journal 4, 222–231.

Gefen, A., 2008. Bioengineering models of deep tissue injury. Advances in Skin and Wound Care 21, 30–36.

Hendriks, F.M., Brokken, D., van Eemeren, J.T., Oomens, C.W., Baaijens, F.P., Horsten, J.B., 2003. A numerical-experimental method to characterize the non-linear mechanical behaviour of human skin. Skin Research and Technology 9, 274–283.

Henrot, P., Stines, J., Walter, F., Martinet, N., Paysant, J., Blum, A., 2000. Imaging of the painful lower limb stump. Radiographics 20, S219–S235.

James, A.G., Green, A., Simpson, G.M., 1975. Strain energy functions of rubber I characterization of gum vulcanizates. Journal of Applied Polymer Science 19, 2033–2058.

Jia, X., Zhang, M., Lee, W.C., 2004. Load transfer mechanics between trans-tibial prosthetic socket and residual limb—dynamic effects. Journal of Biomechanics 37, 1371–1377.

Kulkarni, J., Pande, S., Morris, J., 2006. Survival rates in dysvascular lower limb amputees. International Journal of Surgery 4, 217–221.

Lanir, Y., Dikstein, S., Hartzshtark, A., Manny, V., 1990. In-vivo indentation of human skin. Journal of Biomechanical Engineering 112, 63–69.

Le, K.M., Madsen, B.L., Barth, P.W., Ksander, G.A., Angell, J.B., Vistnes, L.M., 1984. An in-depth look at pressure sores using monolithic silicon pressure sensors. Plastic and Reconstructive Surgery 74, 745–756.

Lee, W.C., Zhang, M., Jia, X., Cheung, J.T.M., 2004. Finite element modeling of the contact interface between transtibial residual limb and prosthetic socket. Medical Engineering and Physics 26, 655–662.

Linder-Ganz, E., Gefen, A., 2007. The effects of pressure and shear on capillary closure in the microstructure of skeletal muscles. Annals of Biomedical Engineering 35, 2095–2107.

Linder-Ganz, E., Engelberg, S., Scheinowitz, M., Gefen, A., 2006. Pressure-time cell death threshold for albino rat skeletal muscles as related to pressure sore biomechanics. Journal of Biomechanics 39, 2725–2732.

Linder-Ganz, E., Shabshin, N., Itzchak, Y., Gefen, A., 2007. Assessment of mechanical conditions in sub-dermal tissues during sitting: a combined experimental-MRI and finite element approach. Journal of Biomechanics 40, 1443–1454.

Lyon, C.C., Kulkarni, J., Zimerson, E., VanRoss, E., Beck, M.H., 2000. Skin disorders in amputees. Journal of American Academy of Dermatology 42, 501–507.

Mak, A.F.T., Zhang, M., Boone, D.A., 2001. State-of-the-art research in lower-limb prosthetic biomechanics—socket interface: a review. Journal of Rehabilitation Research and Development 38, 161–174.

Palevski, A., Glaich, I., Portnoy, S., Linder-Ganz, E., Gefen, A., 2006. Stress relaxation of porcine gluteus muscle subjected to sudden transverse deformation as related to pressure sore modeling. Journal of Biomechanical Engineering 128, 782–787.

Peery, J.T., Klute, G.K., Blevins, J.J., Ledoux, W.R., 2006. A three-dimensional finite element model of the transibial residual limb and prosthetic socket to predict skin temperatures. IEEE Transactions on Neural Systems and Rehabilitation Engineering 14, 336–343.

Portnoy, S., Yarnitzky, G., Yizhar, Z., Kristal, A., Oppenheim, U., Siev-Ner, I., Gefen, A., 2007. Real-time patient-specific finite element analysis of internal stresses in the soft tissues of a residual limb: a new tool for prosthetic fitting. Annals of Biomedical Engineering 35, 120–135.

Quesada, P., Skinner, H.B., 1991. Analysis of a below-knee patellar tendon-bearing prosthesis: a finite element study. Journal of Rehabilitation Research and Development 3, 1–12.

Reihsner, R., Balogh, B., Menzel, E.J., 1995. Two-dimensional elastic properties of human skin in terms of an incremental model at the in vivo configuration. Medical Engineering and Physics 17, 304–313.

Reynolds, D.P., Lord, M., 1992. Interface load analysis for computed-aided design of below-knee prosthetic sockets. Medical and Biological Engineering and Computing 30, 419–426.

Sanders, J.E., Daly, C.H., 1993. Normal and shear stresses on a residual limb in a prosthetic socket during ambulation: comparison of finite element results with experimental measurements. Journal of Rehabilitation, Research and Development 30, 191–204.

Sanders, J.E., Greve, J.M., Mitchell, S.B., Zachariah, S.G., 1998. Material properties of commonly-used interface materials and their static coefficients of friction with skin and socks. Journal of Rehabilitation Research and Development 35, 161–176.

Sanders, J.E., Zachariah, S.G., Jacobson, A.K., Fergason, J.R., 2005. Changes in interface pressures and shear stresses over time on trans-tibial amputee subjects ambulating with prosthetic limbs: comparison of diurnal and six-month differences. Journal of Biomechanics 38, 1566–1573.

Silver-Thorn, M.B., Childress, D.C., 1996. Parametric analysis using the finite element method to investigate prosthetic interface stresses for persons with trans-tibia amputation. Journal of Rehabilitation Research and Development 33, 227–238.

Snedekera, J.G., Barbezatb, M., Niederera, P., Schmidlinc, F.R., Farshad, M., 2005. Strain energy density as a rupture criterion for the kidney: impact tests on porcine organs, finite element simulation, and a baseline comparison between human and porcine tissues. Journal of Biomechanics 38, 993–1001.

Steege, J.W., Schnur, D.S., Childress, D.S., 1987. Prediction of pressure in the below-knee socket interface by finite element analysis. ASME Symposium on the Biomechanics of Normal and Pathological Gait, 39–44.

Stekelenburg, A., Oomens, C.W., Strijkers, G.J., de Graaf, L., Bader, D.L., Nicolay, K., 2006a. A new MR-compatible loading device to study in vivo muscle damage development in rats due to compressive loading. Medical Engineering and Physics 28, 331–338.

Stekelenburg, A., Oomens, C.W., Strijkers, G.J., Nicolay, K., Bader, D.L., 2006b. Compression-induced deep tissue injury examined with magnetic resonance imaging and histology. Journal of Applied Physiology 100, 1946–1954.

Stekelenburg, A., Strijkers, G.J., Parusel, H., Bader, D.L., Nicolay, K., Oomens, C.W., 2007. Role of ischemia and deformation in the onset of compression-induced deep tissue injury: MRI-based studies in a rat model. Journal of Applied Physiology 102, 2002–2011.

Tonuk, E., Silver-Thorn, M.B., 2004. Nonlinear viscoelastic material property estimation of lower extremity residual limb tissues. Journal of Biomechanical Engineering 126, 289–300.

Zachariah, S.G., Sanders, J.E., 2000. Finite element estimates of interface stress in the trans-tibial prosthesis using gap elements are different from those using automated contact. Journal of Biomechanics 33, 895–899.

Zhang, M., Roberts, C., 2000. Comparison of computational analysis with clinical measurement of stresses on below-knee residual limb in a prosthetic socket. Medical Engineering and Physics 22, 607–612.

Zhang, M., Lord, M., Turner-Smith, A.R., Roberts, V.C., 1995. Development of a nonlinear finite element modeling of the below-knee prosthetic socket interface. Medical Engineering and Physics 17, 559–566.

Zhang, M., Turner-Smith, A.R., Tanner, A., Roberts, V.C., 1998. Clinical investigation of the pressure and shear stress on the trans-tibial stump with a prosthesis. Medical Engineering and Physics 20, 188–198.